PHYSICAL REVIEW B, VOLUME 65, 140404(R)

Comparison of experimental and numerical micromagnetic dynamics in coherent precessional switching and modal oscillations

W. K. Hiebert,* G. E. Ballentine, and M. R. Freeman
Department of Physics, University of Alberta, Edmonton, Alberta, Canada T6G 2J1
(Received 15 October 2001; published 28 March 2002)

Spatiotemporally resolved experimental vector magnetometry is combined with time-domain numerical micromagnetic simulation to investigate two, precessional-based, dynamic processes in thin-film magnetic elements. Large angle (>180°), ultrafast, magnetization vector motions compare well between experiment and simulation and constitute a direct observation of nearly-ideal precessional switching. High-frequency spin-wave generation is inferred by apparent reduction in the magnetization vector length. Small angle (<1°) nonequilibrium modal oscillations in ferromagnetic resonance are compared and show considerable agreement in the long-wavelength magnetic spatial structure.

DOI: 10.1103/PhysRevB.65.140404 PACS number(s): 75.50.Ss, 68.37.Ef, 77.80.Fm, 78.47.+p

The dynamical motions of magnetization on small length and fast time scales are fundamental to studies in magnetism. Understanding magnetic switching[1,2] (the polarity reversal of a magnetic element or bit), which forms the basis of magnetic recording and magnetoelectronics,[3,4] requires detailed knowledge of these magnetic motions. In particular, recent experimental attention has centered on coherent precessional switching,[5–9] a phenomenon whose direct observation has remained elusive, as the fastest avenue towards reversal.

Numerically, micromagnetic simulation[10–13] has seen tremendous progress towards understanding the dynamics. Experimentally, ultrafast magneto-optic imaging[14,15] has given spatiotemporal experimental access to the nonequilibrium magnetic states.[16–22] The confluence of these two approaches holds great promise for new insight into magnetization dynamics.

In this paper, we report comparison of time-domain experimental and simulated numerical data in elucidating micromagnetic dynamics. In a large angle regime (>180°), magnetization motions are spatiotemporally and vectorially resolved in a direct, though diffraction limited, ''experimental micromagnetic'' observation of coherent precessional switching. Presentation of the experimental data in micromagnetic vector maps allows direct comparison to the single damping parameter modeling, which shows satisfactory agreement. Apparent reduction in the magnetization vector length suggests high-spatial frequency spin-wave generation during the ''coherent'' process. In a small angle regime (<1°), similar nonequilibrium spatial patterns of small amplitude modal oscillations in ferromagnetic resonance are captured in simulation and experiment. The value inherent in the ability to compare to experimental images is seen as the importance of an external field gradient is deduced and additional confidence in the simulation invites conjecture on high-resolution spatial structure in the experiment.

The experimental procedure[23,24] combines an ultrafast laser with a scanning optical microscope to stroboscopically image the nonequilibrium magnetization states via magneto-optic Kerr effect interactions at the sample surface. Signal is phase-sensitively detected by low-frequency gating and a quadrant detection scheme is used to decouple and simultaneously measure all three magnetization vector components. Time resolution is 50 ps (trigger limited) and spatial resolution is 0.65 μm (diffraction limited). The numerical simulation is a time-domain two-dimensional, finite-element calculation[10–13] of the Landau Lifshitz Gilbert equation with effective magnetic field containing external, exchange, crystalline anisotropy, and magnetostatic contributions. The field is calculated using fast Fourier transform methods and the equation integrated with a fourth-order Runge-Kutta method and variable time stepper. The damping constant α is taken to be 0.008 and the saturation magnetization of permalloy taken to be $4\pi M_s = 10.8$ kOe (obtained from ferromagnetic resonance oscillation fits from Ref. 16). The cell size is 15 nm×15 nm.

The first set of results (Fig. 1), show a large angle precessional process[23] (also available in animated form through EPAPS[25]). This is the vectorial spatiotemporal magnetization response at the end of the application of a bipolar, square, in-plane field pulse to a stadium-shaped permalloy element [shown in the SEM micrograph in Fig. 1(a)]. The easy axis and magnetic field applications are along the x axis shown in perspective Fig. 1(b). The sample is immersed in a static magnetic field of +100 Oe (along $+x$), with a 10 ns long, 1/2 ns rise and 1 ns fall time magnetic field pulse of −160 Oe (along $-x$) created by a lithographic current line directly underneath the sample.

The images in (c) are 100 ps spaced frames capturing the precessional switching just after the field condition changes from $\mathbf{H}(t_0) = -60$ Oe to $\mathbf{H}(t_1) = +100$ Oe. In each frame, the three-component micromagnetic vector data is represented by cones depicting the magnetization direction. The size of the cones and the gray scale background beneath correspond with the length of vector $|\mathbf{M}|$, as deduced from its components measured under the focus spot of the laser.[26] The experimental data is on the left and the numerical is on the right.[27] Initially (in −60 Oe field), the spins lie along the negative x axis, slightly canted along the negative y axis (not shown—see movies[25]), after near-equilibration following the reversal process due to the front edge of the square pulse.

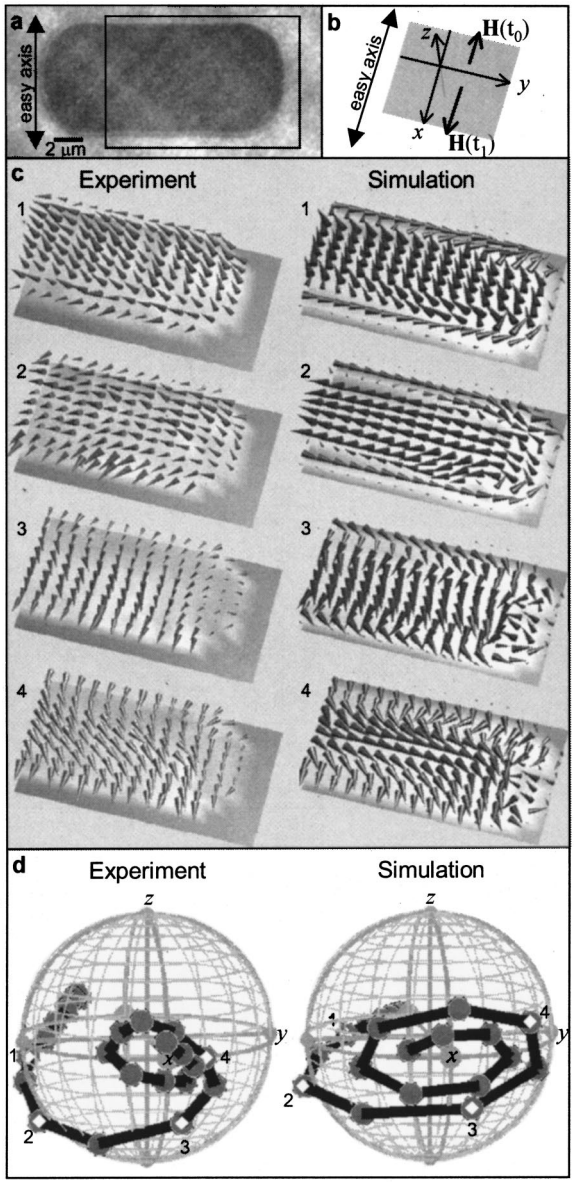

FIG. 1. Experimental and numerical comparison of a large angle precessional magnetic switching process. (a) The stadium shaped 15 nm thick $Ni_{80}Fe_{20}$ sample with scan area and easy axis shown. (b) The coordinate system and magnetic field application geometries. The external field changes from $\mathbf{H}(t_0) = -60$ Oe to $\mathbf{H}(t_1) = +100$ Oe to initiate the switching process shown in (c). (c) 100 ps spaces vector image frames capturing the large angle precessional switch, compared between experiment and simulation. (d) Locus of points indicating the average magnetization trajectory. The points are 50 ps apart and the corresponding numbered frames in (c) are pinpointed by diamonds ($\diamond$). The trajectory starts on the back half of the sphere and crosses the *y*-*z* plane before settling into resonance about the *x* axis.

The shape of the element effectively defines an extra magnetic field along the long axis of the sample. As the external field condition changes to +100 Oe, the magnetization further relaxes toward the *y* direction (frame 1), then starts a fairly uniform ''rotation-in-unison'' reversal process due to the torque coupling to the *y* component. The torque drives the magnetization down out of the *x*-*y* plane creating the demagnetizing field that propels it through reversal towards the $+x$ axis (frames 2–4) in the ''ideal precessional reversal.'' [1,2] As the demagnetizing field falls off, the magnetization continues a damped resonant oscillation[25] around the equilibrium direction ($+x$ axis).

The unit spheres in Fig. 1(d) show this gyrotropic switching process clearly as the locus of points traced by the orientation of the magnetization vector at 50 ps intervals over the course of the reversal. Note that the points start on the back half of the sphere and cross the *y*-*z* plane before settling into resonance about *x*. As the vector crosses the *y*-*z* plane, the points become more widely spaced on the surface of the unit sphere owing to the additional demagnetizing field contribution (giving rise to a higher precession rate). In addition, the vector size shrinks during the crossing of the *y*-*z* plane, as reflected by the gray-scale background in Fig. 1(c). Even in this mostly uniform motion, there is a signature of short wavelength changes beyond the experimental spatial resolution, as some Zeeman energy is transferred into exchange and some spin waves generated.[28–30] Including spatial averaging of the numerical data,[27] the simulation also shows this dip in magnetization, signaling this energy transfer as the large angle motion proceeds.

While these agreements are encouraging, we are far from stating that coherent magnetization reversal is resolved. The differences between simulation and experiment will be of greatest interest as we proceed. The reversal during front onset of the square pulse (not shown) occurs similarly as the back for numerical data,[23] but the experimental front data are less uniform than their back reversal counterpart. While local precession is still evident on the front slope, it is not coherent across the sample as variable canting in the initial state leads to variable sign of the torque coupling. The back reversal has a non-equilibrium initial state to work off of which may give enough extra energy to propel it into precessional reversal. This would make pinning sites in the real sample less important for the back reversal, thus giving better agreement with the single crystal simulation.

Moving to smaller precessional motions, magnetostatic wave oscillation data is compared in Fig. 2. The experimental data is from an 8 μm diameter Permalloy ($Ni_{80}Fe_{20}$) disk of 100 nm thickness, shown in the SEM image in Fig. 2(a) (easy axis in the horizontal direction).[16,31,32] The static magnetic field $\mathbf{H}_{dc}$ of 250 Oe applied along the easy axis (two orders of magnitude above the coercivity) fully saturates the sample except for small flux closure patterns at the left and right edges. An out-of-plane transient magnetic field pulse, provided by a fast electrical current pulse through the one-turn lithographic gold loop shown in the SEM image, excites the disk into small angle precessional magnetization oscillations. The temporal shape of this magnetic field pulse is shown schematically in Fig. 2(b), along with its spatial dependence over the area inhabited by the disk, calculated using the Biot-Savart law. The features of most importance in the temporal shape are those containing high enough frequency components to feed energy to magnetic oscillations (two upward slopes) centered around 550 and 1100 ps, respectively.

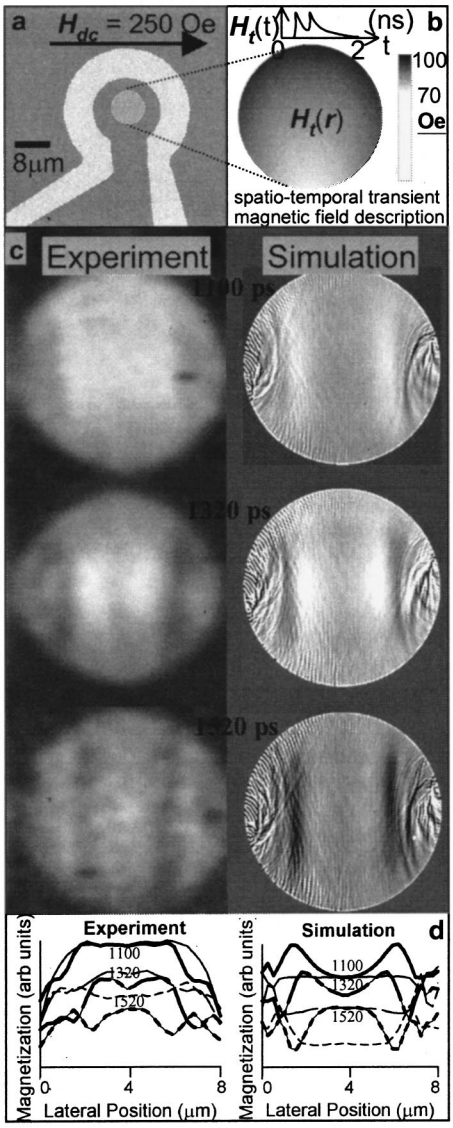

FIG. 2. Experimental and numerical comparison of spatially nonuniform ferromagnetic resonance in a $Ni_{80}Fe_{20}$ disk. (a) Scanning electron micrograph of the disk in a transient magnetic field excitation coil. A permanent magnetic field $\mathbf{H}_{dc}$ is applied along the horizontal axis. (b) Spatiotemporal description of the transient magnetic field $\mathbf{H}_t$. A temporal trace cartoon depicts the double-peaked transient nature of $\mathbf{H}_t$ while the spatial dependence (at maximum field) is shown, calculated from the coil geometry using the Biot-Savart law. (c) Direct comparison of the resonant modes of the out-of-plane magnetization component imaged by time-resolved microscopy and calculated by time-domain simulation. The magnetically saturated sample is excited into the small angle modes by the transient field $\mathbf{H}_t$. (d) Averaged, horizontal line traces of the out-of-plane magnetization component from (c) (darker lines) and the corresponding traces from successive peaks after a single pulse excitation (lighter lines). Modes with four local maxima are amplified by the second field pulse (more so in the simulated data).

The results are shown in Fig. 2(c): three ''snapshot'' frames at times shortly after the second excitation. A gray scale map (of the out-of-plane magnetization component) with a narrow contrast range (a few percent of M_s) is used here since it is more informative visually than vector data for these small angle motions. The rich structure arises from extra energy pumped in by the second excitation while the system is already in a nonequilibrium state from its first excitation. The agreement between experiment and simulation is compelling. The ''unsaturated spins'' in the closure areas at the left and right edges lead the resonant oscillations, and the symmetry is well matched between experiment and simulation.

Magnetic modes in the sample can only be excited by a gradient in the effective field. In the simulation, the gradient produced by the internal field due to dipole-dipole coupling (sample shape magnetostatics) did not by itself produce satisfactory modal agreement. It was necessary to accurately incorporate the spatial variation of the transient magnetic field to reproduce the magnetic structure shown in the experiment. This variation across the sample shape must be important in determining and/or ''amplifying'' the modes that become excited in the system. Additionally, simulations done with the exchange constant reduced from $1.05*10^{-6}$ erg/cm (the value for polycrystalline permalloy) to $5.25*10^{-7}$ erg/cm confirm the dominance of dipole fields (through the sample shape) over exchange in defining the spatial response. The well-matched simulation subsequently yields a complementary advantage by allowing further interpretation of the experimental. This is demonstrated near the edges; the high spatial frequencies and complex response visible in numerical data is not captured in the spatial bandwidth-limited experiment (the patches of ''gray'' at left and right edges). These two areas, with the most complex initial conditions and quickest response to external magnetic field changes, again provide an example of large energy transfer to nonlinear high spatial frequency spin waves.[28–30] The experimental signature of this transfer in this instance (as well as in Fig. 1) are the ''patches of gray,'' spatially averaged by the limited optical resolution.

Finally, a comparison of the mode profiles with (darker lines) and without (lighter lines) a second magnetic field pulse ''kick'' is shown in Fig. 2(d). In the experimental data, modes with four local maxima are barely evident after the single kick. These modes are amplified after the second current pulse (a similar before and after amplification is evident in Fig. 3 of Ref. 32). This amplification effect is more pronounced in the simulated data. The temporal separation of the two current pulses, at 550 ps, is about 2.6 ferromagnetic resonant wavelengths, making the second neither completely constructive nor destructive to the resonant mode.

In conclusion, we have presented a comparison of experimental and numerical data of two micromagnetic dynamic precessional-based processes in magnetic elements. In the large angle, the first direct observation of coherent precessional switching was reported with satisfactory agreement to modeling and high-spatial frequency spin-wave generation detected during the coherent process. The small angle case gave agreement and insight into modal ferromagnetic resonance oscillations and demonstrated the significance of a tandem approach of experiment and simulation.

Note added in proof. We have recently learned of related work by Rasing *et al.*[33]

We thank A. Stankiewicz for groundwork in the experiment and simulation and L. Lagae for assistance with the measurements. This work was supported by the Natural Sciences and Engineering Research Council, the Canadian Institute for Advanced Research, the National Storage Industry Consortium, and the Province of Alberta. The numerical work was performed using the Multimedia Advanced Computational Infrastructure at the University of Alberta.

*Present address: IMEC, Kapeldreef 75, B-3001 Leuven, Belgium; Email address: hiebert@imec.be

[1] D. O. Smith, in *Magnetism*, edited by G. T. Rado and H. Suhl (Academic Press, New York, 1963), Vol. III, pp. 465–523.
[2] W. D. Doyle, S. Stinnet, C. Dawson, and L. He, J. Magn. Soc. Jpn. **22**, 91 (1998).
[3] G. A. Prinz, Science **282**, 1660 (1998).
[4] J. De Boeck and G. Borghs, Phys. World **12** (4), 27 (1999).
[5] Y. Acremann *et al.*, Science **290**, 492 (2000).
[6] M. Bauer, R. Lopusnik, J. Fassbender, and B. Hillebrands, Appl. Phys. Lett. **76**, 2758 (2000).
[7] T. M. Crawford, P. Kabos, and T. J. Silva, Appl. Phys. Lett. **76**, 2113 (2000).
[8] C. H. Bach *et al.*, Science **285**, 864 (1999).
[9] R. H. Koch *et al.*, Phys. Rev. Lett. **81**, 4512 (1998).
[10] M. Mansuripur, J. Appl. Phys. **63**, 5809 (1988).
[11] N. Hayashi, T. Inoue, Y. Nakatani, and H. Fukushima, IEEE Trans. Magn. **24**, 3111 (1988).
[12] B. Yang and D. R. Fredkin, J. Appl. Phys. **79**, 5755 (1996).
[13] H. N. Bertram and J-G. Zhu, in *Solid State Physics*, edited by H. Ehrenreich and D. Turnbull (Academic Press, New York, 1996), Vol. 46, pp. 271–371.
[14] M. Kryder and F. B. Humphrey, J. Appl. Phys. **38**, 829 (1969).
[15] D. D. Awschalom *et al.*, Phys. Rev. Lett. **55**, 1128 (1985).
[16] W. K. Hiebert, A. Stankiewicz, and M. R. Freeman, Phys. Rev. Lett. **79**, 1134 (1997).
[17] R. J. Hicken and J. Wu, J. Appl. Phys. **85**, 4580 (1999).
[18] T. M. Crawford, T. J. Silva, C. W. Teplin, and C. T. Rogers, Appl. Phys. Lett. **74**, 3386 (1999).
[19] G. Ju *et al.*, J. Appl. Phys. **87**, 5974 (2000).
[20] G. E. Ballentine, W. K. Hiebert, A. Stankiewicz, and M. R. Freeman, J. Appl. Phys. **87**, 6830 (2000).
[21] B. C. Choi *et al.*, Phys. Rev. Lett. **86**, 728 (2001).
[22] T. J. Silva, C. S. Lee, T. M. Crawford, and C. T. Rogers, J. Appl. Phys. **85**, 7849 (1999).
[23] W. K. Hiebert, Ph.D. thesis, University of Alberta, Canada, 2001. http://laser.phys.ualberta.ca/~hiebert/thesis.html
[24] M. R. Freeman and W. K. Hiebert, in *Spin Dynamics in Confined Magnetic Structures*, edited by B. Hillebrands and K. Ounadjela, (Springer-Verlag, Berlin, 2001).
[25] See EPAPS Document No. E-PRBMDO-65-R02214 for supplemental movies. This document may be retrieved via the EPAPS homepage (http://www.aip.org/pubservs/epaps.html) or from ftp.aip.org in the directory /epaps/. See the EPAPS homepage for more information.
[26] Experimental magnetization component error is about 10% of saturation giving a 7° tilt angle uncertainty and a 10% $|\mathbf{M}|$ length uncertainty
[27] The numerical data here has been treated with the same ''algorithm'' that is applied to the experimental data by virtue of finite spatial resolution in the optical interaction. A 2D Gaussian function of the same diameter as the laser focus spot is convolved with the raw numerical data and only every ~20th point is used (to reduce the sampling density of points to that of the experiment's raster scan). As an averaging element, this convolution allows the length of magnetization to fall below 1 in the numerical data shown. Both experimental and numerical data are shown at only quarter density of sampled points to ease interpretation. Additionally, the *z* component in these data has been exaggerated by a factor of 5 to make more apparent the precessional nature of the reversal.
[28] P. Kabos, S. Kaka, S. E. Russek, and T. J. Silva, IEEE Trans. Magn. **36** (5), Part 1, 3050 (2000).
[29] H. Suhl, IEEE Trans. Magn. **34**, 1834 (1998).
[30] V. L. Safonov and H. N. Bertram, J. Appl. Phys. **85**, 5072 (1999).
[31] W. K. Hiebert, MSc thesis, University of Alberta, Canada, 1998.
[32] M. R. Freeman, W. K. Hiebert, and A. Stankiewicz, J. Appl. Phys. **83**, 6217 (1998).
[33] Th. Rasing *et al.*, Nature (London) (to be published).